Intestinal Stem Cell Niche Defects Result in Impaired 3D Organoid Formation in Mouse Models of Crohn's Disease-like Ileitis

Ludovica F. Buttó,[1,3] Adam Pelletier,[2] Shyam K. More,[5] Nan Zhao,[1] Abdullah Osme,[1,2] Christopher L. Hager,[4] Mahmoud A. Ghannoum,[4] Rafick-Pierre Sekaly,[2] Fabio Cominelli,[1,2,3,6,*] and Maneesh Dave[1,3,5,6,*]

[1]Department of Medicine, Case Western Reserve University School of Medicine, University Hospitals Cleveland Medical Center, 11100 Euclid Avenue, Cleveland, OH 44106-5066, USA
[2]Department of Pathology, Case Western Reserve University School of Medicine, Cleveland, OH 44106, USA
[3]Department of Digestive Health Research Institute, Case Western Reserve University School of Medicine, Cleveland, OH 44106, USA
[4]Center for Medical Mycology, Case Western Reserve University School of Medicine, Cleveland, OH 44106, USA
[5]Division of Gastroenterology & Hepatology University of California Davis, School of Medicine, Institute for Regenerative Cures, 2921 Stockton Boulevard, Suite 1615, Sacramento, CA 95817, USA
[6]Co-senior author
*Correspondence: fabio.cominelli@case.edu (F.C.), mdave@ucdavis.edu (M.D.)
https://doi.org/10.1016/j.stemcr.2020.06.017

SUMMARY

Intestinal epithelial barrier dysfunction is a risk factor in the pathogenesis of Crohn's disease (CD); however, no corrective FDA-approved therapies exist. We used an enteroid (EnO)-based system in two murine models of experimental CD, SAMP1/YitFc (SAMP) and TNF$^{\Delta ARE/+}$ (TNF). While severely inflamed SAMP mice do not generate EnOs, "inflammation-free" SAMP mice form EnO structures with impaired morphology and reduced intestinal stem cell (ISC) and Paneth cell viability. We validated these findings in TNF mice concluding that inflammation in intestinal tissues impedes EnO generation and suppressing inflammation by steroid administration partially rescues impaired formation in SAMP mice. We generated the first high-resolution transcriptional profile of the SAMP ISC niche demonstrating that alterations in multiple key pathways contribute to niche defect and targeting them may partially rescue the phenotype. Furthermore, we correlated the defects in formation and the rescue of EnO formation to reduced viability of ISCs and Paneth cells.

INTRODUCTION

Crohn's disease (CD), a subtype of inflammatory bowel disease (IBD), is characterized by a relapse-remitting, discontinuous, and transmural immunopathology of the gastrointestinal tract that primarily affects the terminal ileum in more than 70% of patients (Baumgart and Sandborn, 2012). The continuous global increase in both incidence and prevalence of IBD rates over the last two decades has affected more than three million adults in the US alone (Dahlhamer et al., 2016; Ng et al., 2018). The pathogenesis of CD is thought to reflect a complex interplay between environmental factors, the gut microbiota and host genetics with intestinal epithelial barrier dysfunction (IEBD) considered an important risk factor. To date, however, there are no FDA-approved corrective IEBD therapies available (Odenwald and Turner, 2017). Therefore, identification of a biologically relevant model to study IEBD and test novel corrective therapies are of great importance in the field of IBD.

Throughout the gastrointestinal tract, a continuous layer of single epithelial cells, derived from a common progenitor LGR5$^+$ intestinal stem cell (ISC), act as the essential barrier, between host immune systems and luminal content (Odenwald and Turner, 2017). Recent advances in 3D intestinal culture techniques have allowed generation of both human and murine intestinal organoids for disease

modeling (Fatehullah et al., 2016; Middendorp et al., 2014; Sato and Clevers, 2013). However, there are limited data indicating whether small intestinal organoids (enteroids [EnOs]), which are composed of only epithelial cells, can recapitulate features of multifactorial CD (Dave et al., 2014; VanDussen et al., 2015; Yoo and Donowitz, 2019).

SAMP1/YitFc (SAMP) mice are a unique model of IBD that spontaneously develop CD-like ileitis that closely resembles human CD, with regard to location, histologic features, and extra-intestinal manifestations. SAMP mice present with discontinuous areas of "cobble-stoning" and transmural inflammation located between areas of normal (healthy) gut mucosa within the terminal ileum (Kosiewicz et al., 2001; Pizarro et al., 2011; Rodriguez-Palacios et al., 2015). Disease occurs in mice with 100% penetrance, within a well-defined time course and is characterized by a "pre-ileitis" phase (at <10 weeks old), and a "chronic, established ileitis" phase ($\geq$25 weeks old), and is responsive to standard CD therapies, such as anti-tumor necrosis factor alpha (anti-TNF-α) drugs and steroids (e.g., dexamethasone) (Marini et al., 2003; Rodriguez-Palacios et al., 2015). SAMP mice exhibit small intestine epithelial barrier dysfunction before ileitis onset that eventually leads to infiltration of active and chronic immune cells in the ileum (Kosiewicz et al., 2001; Olson et al., 2006).

TNF$^{\Delta ARE/+}$ (TNF) mice are a genetically driven model of CD-like ileitis characterized by their continuous, aberrant
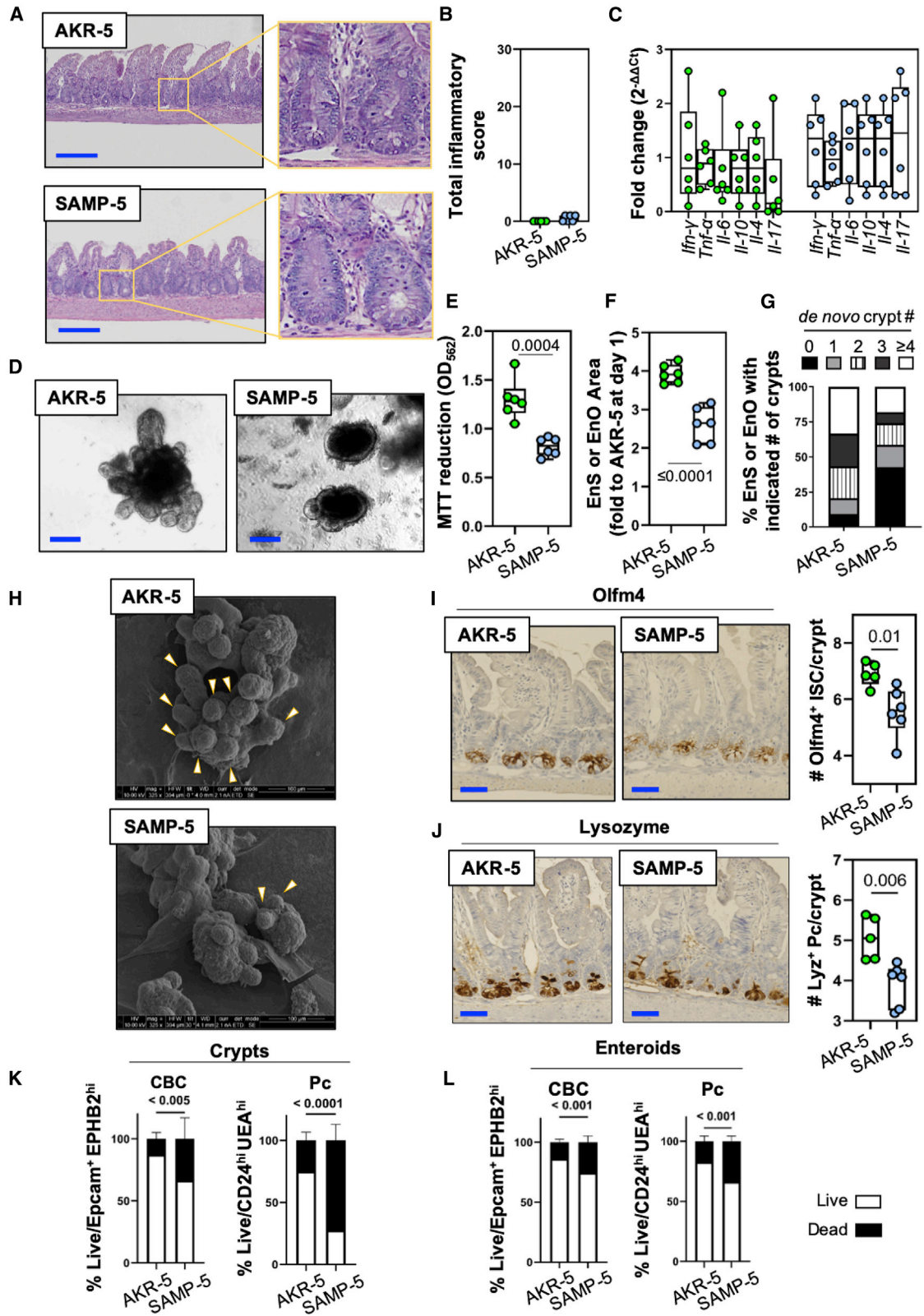
(legend on next page)

production of TNF-α resulting in intestinal inflammation that is demonstrated as early as birth (Kontoyiannis et al., 1999). TNF mice bear a deleted repetitive AU-rich motif in the 3′-untranslated region of the TNF-encoding gene. The resulting aberrant TNF production due to enhanced *Tnf* mRNA stability leads to the development of spontaneous inflammation in the terminal ileum (Baur et al., 2011; Kontoyiannis et al., 1999). Intestinal disease in TNF heterozygotes is characterized by early villous blunting with severe patchy terminal ileitis by 8 weeks of age, and acute and chronic transmural inflammation by 16 weeks, with older mice (5–7 months) displaying loss of villous architecture and granuloma development (Baur et al., 2011; Kontoyiannis et al., 1999; Roulis et al., 2016). Of interest, the selective overexpression of TNF only in the intestinal epithelium appears sufficient to trigger CD-like ileitis (Roulis et al., 2011), indicating that epithelium plays an important role in inflammation pathogenesis in TNF mice.

Herein, we sought to determine whether organoids can recapitulate features of CD in two different mouse models of CD-like ileitis (SAMP and TNF mice), each having high clinical relevance to human disease.

RESULTS

Enteroid Formation Is Impaired in Inflammation-free SAMP Mice

SAMP mice harbor multiple susceptibility loci on chromosomes 6, 9, and X responsible for the epithelial change and immune regulatory functions (Kozaiwa et al., 2003), which together may lead to IEBD preceding onset of histologic inflammation (Olson et al., 2006; Vidrich et al., 2005). To determine whether defect in EnO formation exists and design an *in vitro* model to closely mimic the pathophysiology of CD, we generated enterospheres (EnSs) and EnOs (Stelzner et al., 2012) from young, "inflammation-free" (i.e., pre-ileitis) 5-week-old SAMP (SAMP-5) mice

and age/sex-matched AKR/J parenteral control mice (AKR-5). The terminal ilea of AKR-5 and SAMP-5 mice had normal histology (i.e., no acute inflammation, chronic inflammation, or villous blunting; Figures 1A and 1B), along with no increase of proinflammatory cytokines (Figure 1C) compared with control AKR mice. SAMP-5 EnSs and EnOs had defective morphology (Figure 1D), 1.6-fold reduced viability (0.8 ± 0.1 versus 1.3 ± 0.2, $p < 0.0004$; Figure 1E) and 1.5-fold smaller surface area (3.9 ± 0.2 versus 2.6 ± 0.5, $p < 0.0001$; Figure 1F) compared with AKR-5 (Tables S1 and S2). SAMP-5 mice also had on average a 1.9-fold lower number of EnSs and EnOs compared with controls, despite starting from an equal crypt count (Figures S2A–S2D; Table S3). In addition, after 6 days in culture, SAMP-5-generated EnOs were predominantly cyst-like structures with no crypts, whereas approximately 79% of AKR-5 EnOs displayed *de novo* appearance of two or more crypts with a typical multilobulated organization and only 9% having spherical shape (Figure 1G; Table S4). Scanning electron microscopy validated our observation, showing multiple branching AKR-5 EnOs compared with a more rudimentary morphology of SAMP-5 EnOs (Figure 1H).

Finally, we investigated whether SAMP EnO-impaired morphology was due to loss of ISC or Paneth cell viability which supply essential support to ISCs (Sato et al., 2011a, 2011b; Durand et al., 2012). To this end, we studied by immunohistochemistry staining the expression of OLFM4 (ISC marker) and LYSOZYME (Paneth cell marker). Small intestinal sections from SAMP-5 mice displayed reduced numbers of both ISCs (5.5 ± 0.9 versus 7.0 ± 0.4, $p = 0.006$; Figure 1I) and Paneth cells (3.9 ± 0.5 versus 5.1 ± 0.5, $p = 0.01$; Figure 1J) compared with those from AKR-5 mice. We confirmed these observations by flow cytometry adopting a combinational cell surface marker-mediated strategy that allows the purification of a highly enriched and homogeneous population of crypt base columnar (CBC) stem cells, transcriptionally and functionally equivalent to the gold standard Lgr5-GFP ISCs (Nefzger et al.,

Figure 1. Defective EnO Formation in Intestinal Inflammation-free SAMP Mice

Data, indicated as mean ± SD, correspond to three independent experiments (n = 2 mice/group/experiment).

(A) Representative photomicrographs of ileal sections of 5-week-old AKR (AKR-5) and SAMP (SAMP-5) mice. Scale bars, 200 μm. Zoomed images are at 20× magnification.

(B) Total inflammatory score of ileal tissue from AKR-5 (0.0 ± 0.0) and SAMP-5 (0.5 ± 0.5).

(C–F) (C) Relative expression of indicated cytokine mRNA measured in total tissue RNA extracted from 5-week-old SAMP and AKR ilea. The mRNA levels were determined by qRT-PCR, normalized to β-actin and expressed as fold change ($2^{-\Delta\Delta Ct}$). Small intestinal EnSs and EnOs (D) growth, (E) viability, and (F) size from AKR-5 and SAMP-5 mice after 6 days in culture. Scale bars, 100 μm.

(G) Quantification of *de novo* crypt formation at day 6 in EnOs from AKR-5 and SAMP-5 mice.

(H) Scanning electron micrographs of EnOs from AKR-5 and SAMP-5 mice at day 6 in culture. Arrows indicate *de novo* crypts. Note the higher number of *de novo* crypts in EnOs from AKR-5 compared with those from SAMP-5.

(I–L) (I) OLFM4 and (J) LYSOZYME staining of AKR-5 and SAMP-5 small intestinal crypts. Scale bars, 50 μm. Frequency of live and dead crypt base columnar (CBC) stem cells (Epcam$^+$ Ephb2^{hi}/CD44^{hi}GRP78^{low}/CD166$^+$ CD24^{med}/CD31$^-$CD45$^-$) and Paneth cells (CD24^{hi}UEA$^+$/CD31$^-$CD45$^-$) isolated from (K) crypts and (L) EnOs of 5-week-old SAMP and AKR mice.
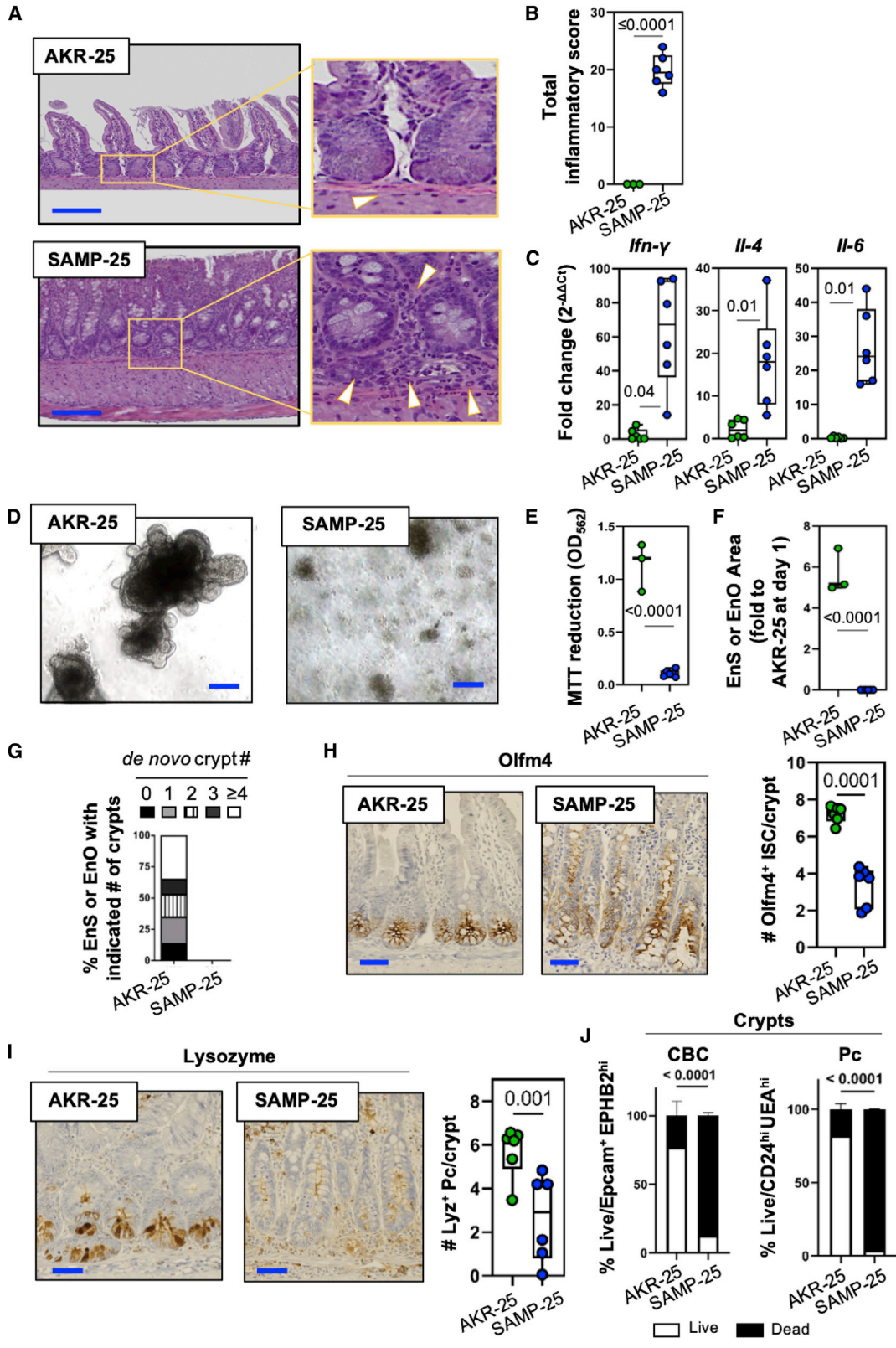
(legend on next page)

2016) (Figures S1D and S1E). CBC and Paneth cells isolated from SAMP-5 crypts (33.4% ± 16.9% versus 12.6% ± 5.2% and 72.3% ± 13.1% versus 24.8% ± 6.6%, p < 0.005; Figure 1K) and EnOs (25.2% ± 5.3% versus 13.7% ± 2.6% and 33.6% ± 4.3% versus 17.0% ± 4.5%, p < 0.01; Figure 1L) exhibited higher percentage of dead cells compared with those from AKR-5 controls. Collectively, these data demonstrate that EnOs from SAMP-5 mice, presenting no histologic inflammation in the ileum, are characterized by impaired formation, defective morphological features, and reduced ISCs and Paneth cell viability compared with those from control AKR mice.

Crypts from the Small Intestine of SAMP Mice with Established Ileitis Do Not Form EnSs and EnOs

To assess the effect of chronic inflammation on the ability to form EnOs, we then generated EnOs from highly inflamed SAMP (25-week-old, SAMP-25) mice, as well as from age-matched AKR controls (AKR-25). Ileal tissues from SAMP-25 mice harbored chronic inflammation, villous blunting, and heavy infiltration of inflammatory cells producing proinflammatory cytokines, i.e., *ifn-γ*, *il-4*, and *il-6* (Figures 2A–2C). Morphologic assessment revealed that, while crypts from AKR-25 mice formed 3D branching EnOs, SAMP-25 crypts from highly inflamed mice were not able to round up to form EnS or EnO structures, and persisted as clusters of single cells that eventually died by day 6 in culture (Figures 2D–2G and S2E–S2H; Tables S1–S4). Small intestine from SAMP-25 mice displayed reduced number of both ISCs (3.3 ± 1.0 versus 7.2 ± 0.5, p = 0.0001; Figure 2H) and Paneth cells (2.7 ± 2.0 versus 5.7 ± 1.2, p = 0.01; Figure 2I) compared with those from AKR-25 mice. In addition, SAMP-25 crypts had a markedly higher percentage of dead cells in CBC stem cell and Paneth cell suspensions compared with control AKR-25 crypts (87.1% ± 2.2% versus 22.8% ± 10.7% and 96.1% ± 0.3% versus 17.5% ± 3.9%, p < 0.0001; Figure 2J). Conversely, colon crypts of SAMP-25 mice were able to round up to form colonospheres (CnSs) leading to colonoid (CnO) formation (Figures S3A–S3C), likely because SAMP mice characteristi-

cally do not exhibit inflammation in the colon, have normal colon barrier function, and the disease is isolated to the small bowel (Olson et al., 2006). Collectively, our data demonstrate that inflammation correlates with reduced number of viable ISCs and Paneth cells, and impairs the ability of crypts to form organoid structures.

Multiple Signaling Pathways Contribute to ISC Niche Defect and Enteroid Formation in SAMP Mice

To further investigate the observed EnO formation defect, we used a high-throughput RNA sequencing (RNA-seq) approach to profile transcriptional ISC niche responses using three independent samples in SAMP and respective parental control (AKR) mouse groups based on a histologically defined total inflammatory score, i.e., SAMP-5 and AKR-25 (inflammation-free), and SAMP-25 ("inflamed") (Figure 3A). To avoid physical disruption of the ISC niche, laser capture microscopy (LCM) was used to retrieve crypts and crypt-surrounding regions of terminal ileal cryosections (Figure S4A). Expression of a total of 15,637 unique genes was detected in SAMP-25 compared with 15,376 and 15,377 in SAMP-5 and AKR-25, respectively (Figure 3B). Differentially expressed gene (DEG) analysis identified a total of 671 and 811 genes differentially expressed between SAMP-5 and -25 ISC niches, and between SAMP-25 and AKR-25 ISC niches, respectively (Figure 3B). To our knowledge, this global gene expression profile analysis is the first to be carried out in the ISC niche of SAMP mice. Unsupervised hierarchical clustering showed clear segregation of the SAMP-25 ISC niche signature compared with AKR-25 mice, while that of SAMP-5 mice exhibited intermediate gene expression dynamics (Figure 3C, top dendrogram). Multiple gene clusters were up- and downregulated exclusively in SAMP-25 ISC niche, suggesting an inflammation-dependent profile (Figure 3C, side dendrogram). Other clusters encompassed genes differentially expressed consistently in the SAMP-5 and SAMP-25 ISC niches compared with that of AKR-25 mice, indicate potential for their specificity as CD susceptibility genes in SAMP mice and thus their involvement in disease onset

Figure 2. Crypts from Inflamed SAMP Mice do Not Form EnSs and EnOs

Data, indicated as mean ± SD, correspond to three independent experiments (n = 1–2 mice/group/experiment).

(A) Representative photomicrographs of ileal sections of 25-week-old AKR (AKR-25) and SAMP (SAMP-25) mice. Scale bars, 200 μm. Zoomed images are at 20× magnification.

(B) Total inflammatory score of ileal tissue from AKR-25 (0.0 ± 0.0) and SAMP-25 (19.8 ± 2.9) mice.

(C–F) (C) Relative expression of indicated cytokine mRNA measured in total tissue RNA extracted from AKR-25 and SAMP-25 ilea. The mRNA levels were determined by qRT-PCR, normalized to β-actin and expressed as fold change ($2^{-\Delta\Delta Ct}$). Small intestinal EnSs and EnOs (D) growth, (E) viability, and (F) size from AKR-25 and SAMP-25 mice after 6 days in culture. Scale bars, 100 μm.

(G) Quantification of *de novo* crypt formation at day 6 in EnOs from AKR-25 and SAMP-25 mice.

(H and I) (H) OLFM4 and (I) LYSOZYME staining of AKR-25 and SAMP-25 small intestinal crypts. Scale bars, 50 μm.

(J) Frequency of live and dead CBC stem cells (Epcam$^+$ Ephb2^{hi}/CD44^{hi}GRP78^{low}/CD166$^+$ CD24^{med}/CD31$^-$CD45$^-$) and Paneth cells (CD24hiUEA$^+$/CD31$^-$CD45$^-$) isolated from ileal crypts of 25-week-old SAMP and AKR mice.
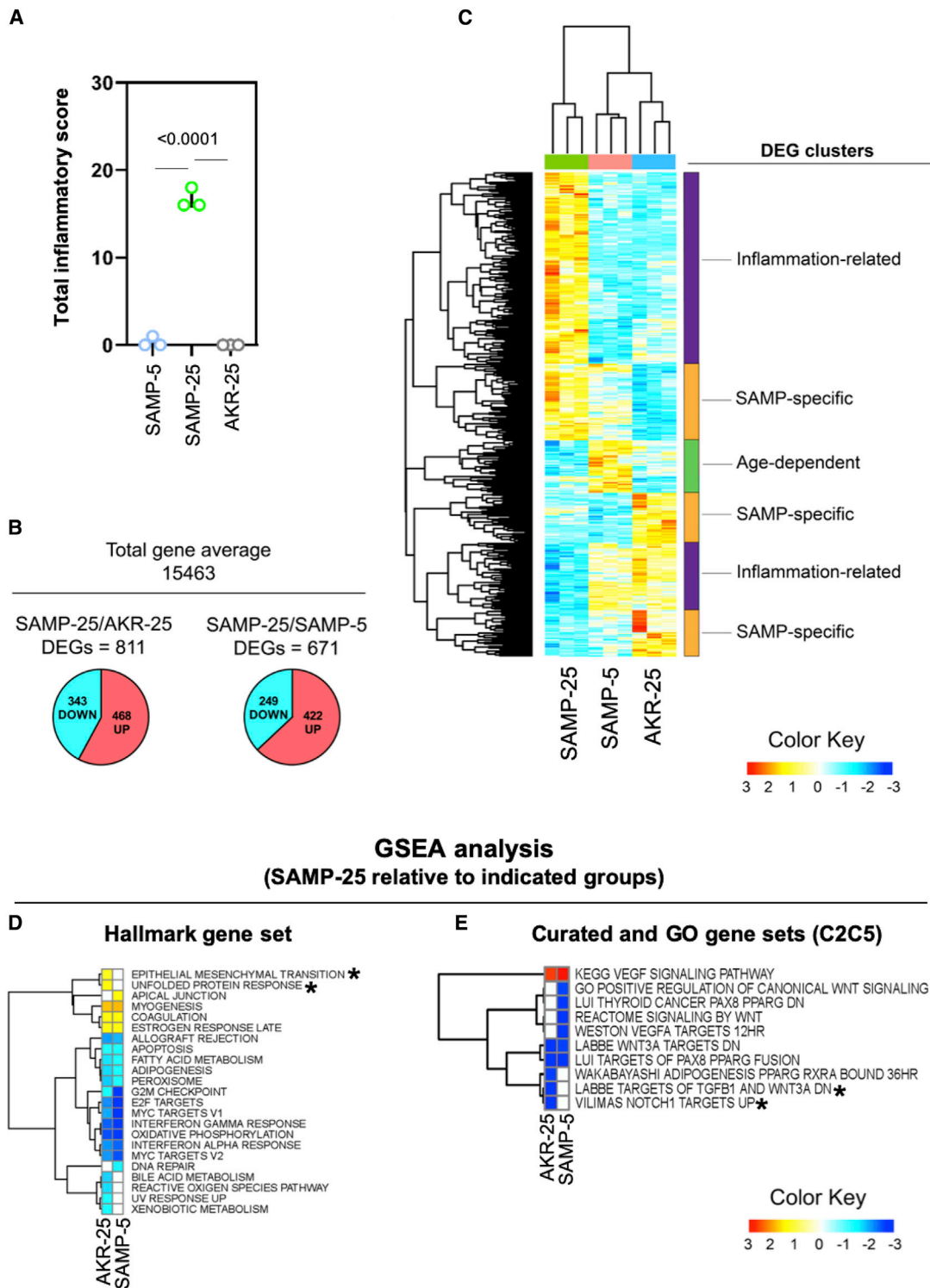
Figure 3. Characterization of Mucosal Gene Expression and Functional Categorization Enrichment of Differentially Expressed Genes in the Ileal ISC Niche of SAMP Mice

Data, indicated as mean ± SD, correspond to three independent experiments (n = 1 mouse/group/experiment).

(A) Total inflammatory score of ileal tissue from AKR-5 (0.0 ± 0.0), SAMP-5 (0.5 ± 0.5), and SAMP-25 (19.8 ± 2.9) mice.

(B) Pie chart indicating differentially expressed genes (DEGs) in the three groups.

(legend continued on next page)

(Figure 3C, side dendrogram). To further delineate DEG function trends, we carried out gene set enrichment analysis (GSEA) and estimated the degree of functional enrichment in pairwise comparisons between SAMP-25 and the other two mice groups. In agreement with data collected from the inflamed ileum of CD patients (Alkim et al., 2015; Severi et al., 2014), the SAMP-25 ISC niche was enriched in genes involved in inflammatory responses (i.e., myogenesis, coagulation, estrogen response, vascular endothelial growth factor signaling, hypoxia, or glycolysis) compared with that of SAMP-5 and AKR-25 mice ($p_{adj} \leq 0.05$, normalized enrichment scores [NES] ≥ 1.3; Figures 3D, 3E, S5A–S5G, and S5H; Table S6). By contrast, other pathways involved in cell metabolism were found depleted in the SAMP-25 ISC niche compared with that of SAMP-5 and AKR-25 mice ($p_{adj} \leq 0.03$, NES ≤ -1.4), including lipid and fatty acid metabolism (adipogenesis, fatty acid metabolism, and peroxisome), cell-cycle metabolism (G2M checkpoint, E2F targets, and MYC targets; apoptosis), cell defense (interferon-γ [IFN-γ], IFN-α), and cellular energy machinery (oxidative phosphorylation and mitochondrial energy metabolism) (Figures 3D, 3E and S5D, S5E; Table S6).

Two signaling pathways, i.e., unfolded protein response (UPR) and epithelial-mesenchymal transition (EMT) pathway, were enriched in the SAMP ISC niche compared with that of the AKR-25 mice, suggestive of Paneth cell defects ($p_{adj} \leq 0.03$, NES ≥ 1.3; Figures 3D, S5B and S5C; Table S6). In contrast, the signaling pathways depleted in the SAMP ISC niche compared with that of AKR-25 mice, were involved in ISC niche homeostasis (Wnt3a and Notch1), antioxidant defense, bile acid metabolism, UV response, and in xenobiotic metabolism ($p_{adj} \leq 0.02$, NES ≤ -1.4; Figures 3D, 3E, and S5F–S5I; Table S6).

Collectively, these data suggest that multiple signaling pathways contribute to ISC niche defect in SAMP mice, and that key biological functions appear to be already altered before inflammation onset and are further dysregulated after inflammation.

Treatment with High Wnt Medium Partially Rescues Organoid Morphology but Not the Molecular Signature in Inflammation-free SAMP Mice
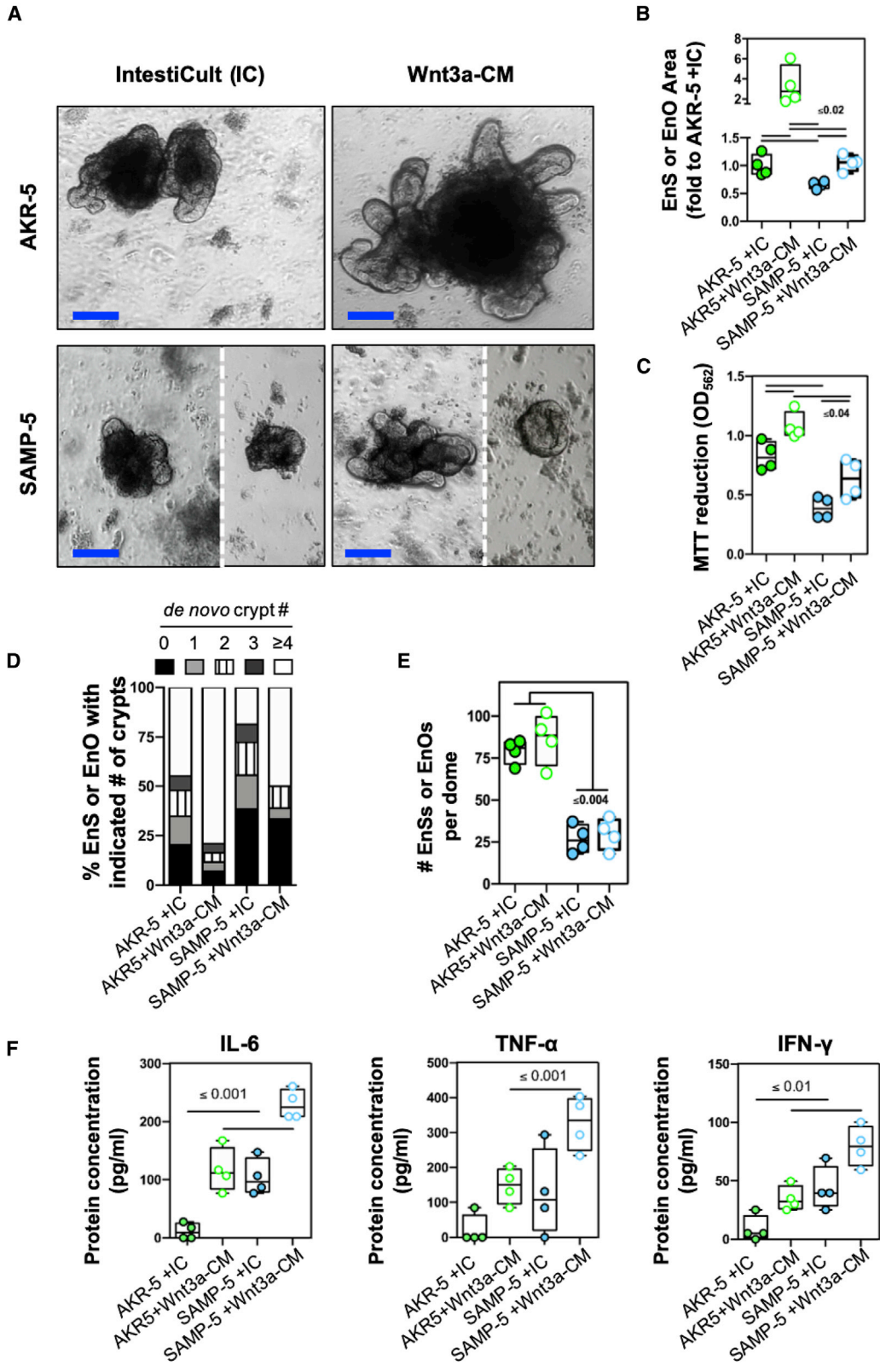
Seminal studies have identified Paneth cells in the ISC niche as a major source of Wnt (Sato et al., 2011a, 2011b; Sato et al., 2009). Considering that Paneth cell viability and function were impaired and Wnt3a signaling pathway was depleted in the SAMP ISC niche compared with that of AKR mice, we investigated whether culturing SAMP crypts in a high Wnt3a-enriched medium (Sato et al., 2011a, 2011b) could restore EnO formation defects. Approximately 40% of SAMP-5 crypts produced simple EnSs, while the remaining crypts generated EnOs characterized by 34% bigger size (1 ± 0.1 versus 0.7 ± 0.1, $p \leq 0.02$; Figures 4A and 4B), 1.6-fold increased viability (0.6 ± 0.2 versus 0.4 ± 0.1, $p \leq 0.04$; Figure 4C), and much more complex branching morphology (Figure 4D), when cultured in high Wnt-3A-conditioned medium (Wnt3a-CM) compared with those expanded in standard Intesticult (IC) medium. These specific morphological phenotypes were retained at passaging. However, generating SAMP-5 crypts in a Wnt3a-CM did not alter the number of EnSs and EnOs generated compared with those obtained in IC medium (Figure 4E). Crypts from AKR-5 control mice generated 3.3-fold bigger EnOs characterized by higher viability and multilobulated structures when cultured in Wnt3a-CM compared with those expanded in IC medium (Figures 4A–4E). Collectively, these data suggest that high Wnt3a-enriched medium partially rescues SAMP-5 EnO morphology, leading to formation of EnOs with size comparable with that of AKR-5 EnOs cultured in IC medium but smaller than AKR-5 EnOs in Wnt3a-CM. Furthermore, crypts from inflamed SAMP-25 mice were not able to round up to form viable EnS or EnO structures in the Wnt3a-CM (data not shown), similarly to those cultured in standard IC medium (Figures 2D–2G), which is likely due to marked cell death of ISCs in SAMP-25 mice.

To gain a better insight into the biological significance of impaired EnO formation observed in *ex vivo* crypt cultures from SAMP-5 mice, we analyzed the expression of genes involved in intestinal secretory cell functions (*Defa1*, *Muc2*, and *Lyz*) in SAMP-5 EnOs cultured in IC and Wnt3a-CM. Regardless of the culturing medium used, the expression of these genes was dysregulated in SAMP-5 EnOs (Figure S5J), suggesting defective function of multiple secretory cell lineages.

Our RNA-seq data indicate that ISC niche defect in SAMP mice is the result of dysregulation in multiple signaling pathways, including inflammation-related pathways. Therefore, we assessed the baseline level of cytokine

(C–E) (C) Heatmap and hierarchical tree comparing differences in gene expression of the top 1,000 DEGs in ISC niche of inflamed SAMP-25 and of inflammation-free (SAMP-5 and AKR-25) mice. Expression values are log2-transformed median-centered fragments per kilobase of transcript per million reads mapped. Red and blue colors represent increased and decreased gene expression compared with ISC niche from inflammation-free mice, respectively. We used a 5% false discovery rate (FDR-adjusted q ≤ 0.05) as the criteria for defining DEGs. Heatmap and hierarchical clustering of shared normalized enrichment scores from GSEA analysis performed on DEGs using (D) Hallmark (MSigDB H) and (E) curated and GO (MSigDB C2C5) signature gene sets in the ISC niche of SAMP-25 versus AKR-25 and SAMP-5 mice, respectively.

A

IntestiCult (IC)   **Wnt3a-CM**

AKR-5

SAMP-5

B

EnS or EnO Area (fold to AKR-5 +IC)

AKR-5 +IC
AKR5+Wnt3a-CM
SAMP-5 +IC
SAMP-5 +Wnt3a-CM

≤0.02

C

MTT reduction (OD$_{562}$)

AKR-5 +IC
AKR5+Wnt3a-CM
SAMP-5 +IC
SAMP-5 +Wnt3a-CM

≤0.04

D

de novo crypt #

0 1 2 3 ≥4

% EnS or EnO with indicated # of crypts

AKR-5 +IC
AKR5+Wnt3a-CM
SAMP-5 +IC
SAMP-5 +Wnt3a-CM

E

EnSs or EnOs per dome

AKR-5 +IC
AKR5+Wnt3a-CM
SAMP-5 +IC
SAMP-5 +Wnt3a-CM

≤0.004

F

IL-6

Protein concentration (pg/ml)

≤ 0.001

AKR-5 +IC
AKR5+Wnt3a-CM
SAMP-5 +IC
SAMP-5 +Wnt3a-CM

TNF-α

Protein concentration (pg/ml)

≤ 0.001

AKR-5 +IC
AKR5+Wnt3a-CM
SAMP-5 +IC
SAMP-5 +Wnt3a-CM

IFN-γ

Protein concentration (pg/ml)

≤ 0.01

AKR-5 +IC
AKR5+Wnt3a-CM
SAMP-5 +IC
SAMP-5 +Wnt3a-CM

(legend on next page)

secretion of EnOs passaged twice revealing that, regardless of the culture medium used, SAMP-5 EnOs produced 2- to 10-fold higher level of interleukin-6 (IL-6), TNF-α, and IFN-γ compared with AKR EnOs (p ≤ 0.01; Figure 4F). Thus, our data show that SAMP-5 EnOs before tissue manifestation of small intestinal inflammation have deficiency of Wnt3a and are able to be rescued by Wnt3a supplementation, albeit partially due to a component of inflammation as well.

Treatment with Dexamethasone Partially Rescues Organoid Morphology in SAMP Mice with Established Ileitis

To investigate whether reduction of inflammation in SAMP-25 mice may correct organoid formation defect, we generated EnOs from SAMP-25 mice treated with dexamethasone (SAMPDex-25). The treatment dramatically reduced inflammation, infiltration of acute and chronic immune cells, and villous blunting compared with non-treated SAMP mice (p ≤ 0.01; Figures 5A–5C). Ileal crypts from SAMPDex-25 mice were able to round up to EnSs and generate viable EnOs (Figures 5D and 5E) with measurable surface area (Figure 5F) and multilobulated structures (Figure 5G and S6A–S6D). However, dexamethasone treatment only partially rescued organoid morphology in SAMP-25 mice, since SAMPDex-25 EnSs and EnOs were, approximately, 50% less viable and 2.5-fold smaller than those from AKR-25 mice (Figures 5E and 5F; Tables S1 and S2). The number of SAMPDex-25 EnSs and EnOs generated from an equal count of seeded crypts was on average 1.3-fold lower than that of AKR-25 mice over 6 days in culture (Figure S6D; Table S3). In addition, SAMPDex-25 EnO cultures displayed a higher recurrence of cyst-like structures and a lower *de novo* appearance of two or more regenerating crypts compared with AKR-25 EnOs (27% versus 13% and 54% versus 65%, respectively) (Figure 5G; Table S4). Small intestines from SAMPDex-25 mice displayed comparable numbers of both ISCs and Paneth cells compared with those from AKR-25 mice, albeit with a decreasing trend (Figures 5H and 5I). Crypts from SAMPDex-25 mice harbored a frequency of dead cells in CBC and Paneth cell populations comparable with that in crypts from control mice, albeit with a decreasing trend (Figure 5J). The frequency of dead cells in CBC and Paneth cell populations was equivalent in EnOs from SAMPDex-25 and AKR-25 mice (Figure 5K), suggesting that dexamethasone treatment rescues EnO formation by enhancing the survival of Paneth cells and ISCs.

It is known that dexamethasone is a potent anti-inflammatory therapeutic agent able to repress nuclear factor κB (NF-κB) transcriptional activation (Barnes, 2017; Stahn et al., 2007). Therefore, we investigated the expression of *Nfkb1* and two other inflammation-induced genes (i.e., *Jak1* and *Mmp9*), which were found by Nanostring analyses to be strongly upregulated (>2- to 7-fold) in the ileum of SAMP mice (Butto et al., 2019). Our data showed that dexamethasone treatment decreased inflammation by downregulating the expression of *Nfkb1*, *Jak1*, and *Mmp9* in the ileum of SAMP mice, restoring gene expression to control mice level (Figure 5L). Interestingly, SAMPDex-25 EnOs continued to show downregulation of *Nfkb1* and *Jak1* expression compared with AKR-25 EnOs (Figure 5M). Overall, these data support the hypothesis that the inflammatory environment of CD negatively alters the ability of intestinal crypts to generate organoid structures. Finally, we demonstrated that reduction of inflammation may rescue EnO morphology in SAMP mice, albeit the recovery is not complete.

Crypts from the Distal Ileum of Young TNF Mice Display Impaired EnO Formation

To confirm the role of inflammation on EnO formation, we used heterozygous TNF mice as a genetically driven murine model for CD-like ileitis (Kontoyiannis et al., 1999). TNF mice continuously produce TNF-α, have evidence of inflammation at birth (Hemmerling et al., 2014). The disease in TNF mice is mostly confined to the terminal ileum, with a *Tnf* mRNA transcript 6- to 40-fold higher than that present in the terminal ileum of control C57BL/6 (BL) mice (Figures 6 and 7C). Notably, sustained TNF-α production is known for inducing apoptosis in intestinal epithelial cell (IEC) and dose-dependent cell death in organoids (Blander, 2016; Grabinger et al., 2014; Kontoyiannis et al., 2002; Roulis et al., 2011).

In light of our data, we used the proximal small intestine (jejunum) in 5- and 25-week-old TNF mice as our corresponding model for small intestinal areas where morphological features of tissue inflammation are absent. Crypts from the distal part of the ileum and from the jejunum of TNF mice at 5 weeks of age (TNFd-5 and TNFp-5, respectively) were isolated and EnOs were generated for comparison analysis to age/sex-matched

---

Figure 4. Wnt3a-Conditioned Medium Partially Rescues EnO Size from SAMP-5 Crypts but Not Dysregulated Molecular Signature

Data, indicated as mean ± SD, correspond to four independent experiments (n = 1 mouse/group/experiment).

(A–E) (A and B) Growth, (C) viability, (D) number, and (E) morphology, quantification of *de novo* crypt formation of 6-day-old EnOs from 5-week-old AKR and SAMP mice cultured in Intesticult (IC) and in Wnt3a-conditioned medium (Wnt3a-CM). Scale bars, 100 μm.

(F) Protein levels of indicated cytokines in AKR-5 and SAMP-5 EnOs cultures in IC or Wnt3a-CM medium. EnOs were passaged twice retaining the observed phenotype.
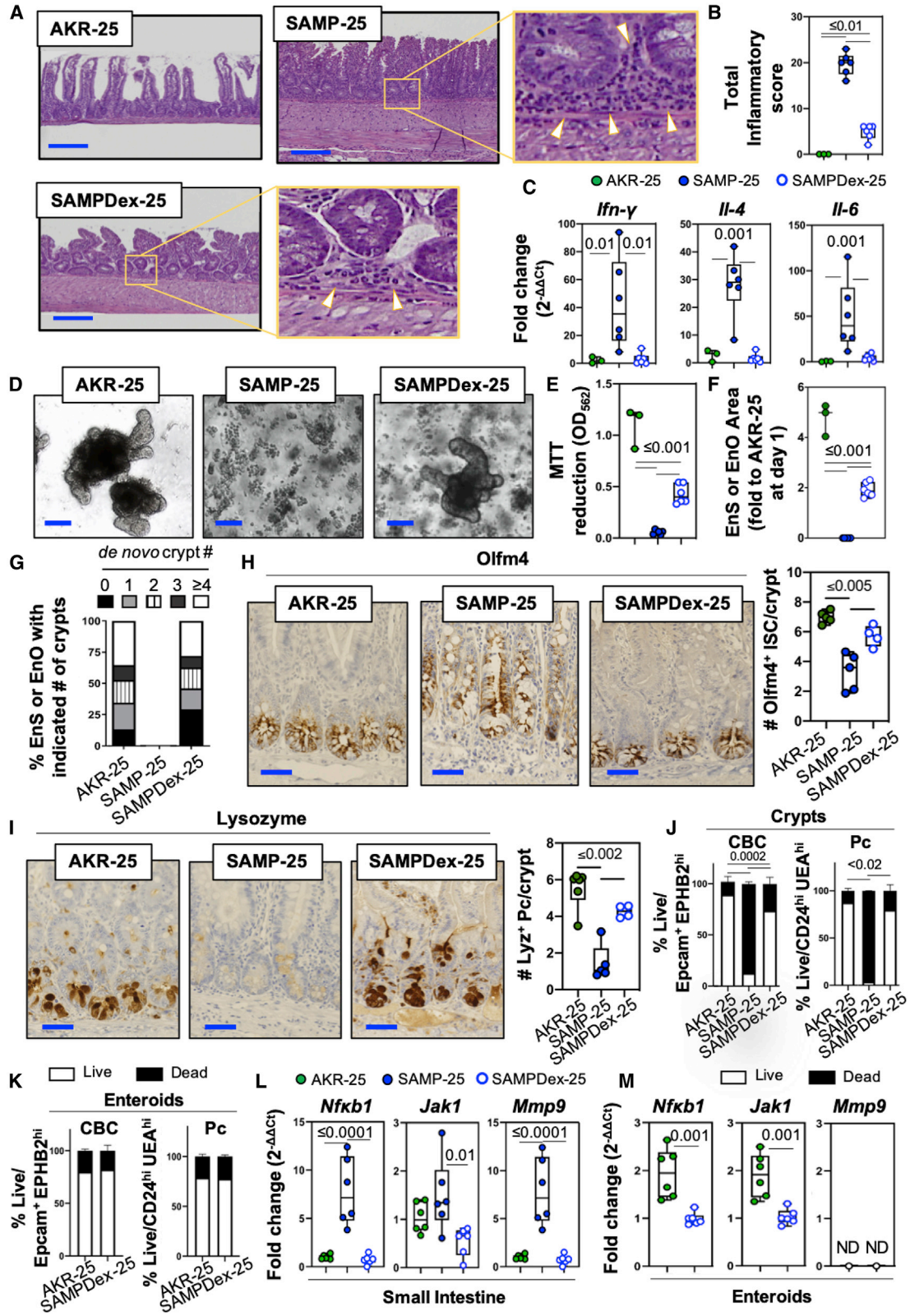
(legend on next page)

inflammation-free control mice (BL-5). TNF mice had no histological evidence of inflammation in the jejunum, although presence of low-grade inflammation in the distal ileum was identified (Figures 6A–6C). Furthermore, the TNFd-5 ileum had nearly 6-fold higher expression of TNF compared with TNFp-5 and BL-5 mice, which corresponded to increased disease severity and impaired ability to form EnOs (Figures 6B and 6C). TNFd-5 mice generated a low yield of rudimentary EnOs, which contrasted the EnOs generated from TNFp-5 and BL-5 mice, which consistently recapitulated the typical multilobulated phenotype, leading to formation of cyst-like budding and branching structures over time (Figure 6D). There was a 57.5% lower viability (Figure 6E) and number of TNFd-5 generated EnSs (2-fold) and EnOs (10-fold) compared with those from TNFp-5 and BL-5 mice (Figures S7A–S7D; Tables S1–S3). Although of similar size (Figures 6F), 58% of the structures generated by TNFd-5 crypts were primarily spherical, in contrast to only 10% from TNFp-5 and BL-5 mice (Figure 6G; Table S4). Distal ileum from TNF-5 mice displayed reduced number of both ISCs (5.0 ± 0.5 versus 7.0 ± 0.0, p = 0.006; Figure 6H) and Paneth cells (3.1 ± 0.5 versus 5.1 ± 0.2, p = 0.005; Figure 6I) compared with that from BL-5 mice. In addition, TNFd-5 crypts and EnOs had a markedly higher percentage of dead cells in CBC stem cell (59.1% ± 13.3% versus 24.3% ± 3.1% and 46.7% ± 7.9% versus 14.6% ± 2.1%, p ≤ 0.02; Figures 6J and 6K) and Paneth cell populations (81.2% ± 12.8% versus 17.6% ± 5.5% and 73.9% ± 8.6% versus 18.7% ± 0.9%, p < 0.0001; Figures 6J and 6K) compared with those from control BL-5 mice.

Our data demonstrate that EnO formation is impaired when crypts are obtained from tissue that has low-grade inflammation with increased TNF, while absence of inflammation in the same tissue (proximal ileum of TNF mice) with normal TNF expression leads to normal EnO formation.

Crypts from the Distal Ileum of Inflamed TNF Mice Are Unable to Form EnOs

To further confirm the role of chronic inflammation in EnO formation, crypts from the distal ileum and jejunum of 25-week-old TNF mice (TNFd-25 and TNFp-25, respectively) were isolated and EnOs were generated and compared with those from controls (BL-25). While pathological features were absent in tissues from TNFp-25 and BL-25 mice, increased infiltration of acute and chronic immune cells, villous blunting phenotype, and high inflammatory score of ileal tissues were detected in TNFd-25 mice (p < 0.0001; Figures 7A and 7B). Furthermore, in this study we demonstrated the segmental differential expression of *Tnf* between the distal and proximal ileum with 7-fold higher expression of *Tnf* in the distal ileum (tissue at 3 cm from the distal part of the ileum versus the proximal part of the ileum at 10 cm) (Figure 7C), which also corresponded to increased disease severity on histological evaluation. Crypts from TNFp-25 and BL-25 mice formed branching EnOs, which equally recapitulated the typical multilobulated phenotype (Figures 7D–7G and S7E–S7H; Tables S1–S4). In contrast, crypts from TNFd-25 mice were 6-fold less viable than those from BL-25 mice, of which few rounded up to form EnSs, and died by day 2 in culture (Figures 7D, 7E, and S7F; Table S1). Distal ileum from TNF-25 mice displayed reduced number of both ISCs (3.4 ± 0.8 versus 6.0 ± 1.0, p = 0.004; Figure 7H) and Paneth cells (1.8 ± 1.8 versus 5.0 ± 0.3, p = 0.007; Figure 7I) compared with those from BL-25 mice. In addition, TNFd-25 crypts had a markedly higher percentage of dead cells in CBC stem cell and Paneth cell populations (67.1% ± 4.1% versus 27.5% ± 8.2% and 84.5% ± 7.1% versus 30.3% ± 4.6%, p < 0.0001; Figure 7J) compared with those from control BL-25 mice.

Considering that, similar to SAMP mice, TNF mice do not develop disease or display inflammation in the colon, TNF-25 colon crypts successfully round up to form CnSs leading

---

Figure 5. Dexamethasone Treatment Partially Rescues EnO Formation in Inflamed SAMP Mice

Data, indicated as mean ± SD, correspond to three independent experiments (n = 1–2 mice/group/experiment).

(A) Representative photomicrographs of ileal sections of 25-week-old dexamethasone-treated SAMP (SAMPDex-25), SAMP (SAMP-25), and AKR (AKR-25) mice. Scale bars, 200 μm. Zoomed images are at 20× magnification.

(B) Total inflammatory score of ileal tissue from SAMPDex-25 (4.8 ± 1.5), SAMP-25 (19.9 ± 2.6), and AKR-25 (0 ± 0) mice.

(C) Relative expression of indicated cytokine mRNA measured in total tissue RNA extracted from SAMPDex-25, SAMP-25, and AKR-25 ilea. The mRNA levels were determined by qRT-PCR, normalized to β-actin and expressed as fold change ($2^{-\Delta\Delta Ct}$).

(D–F) (D) Growth, (E) viability, (F) size, and *de novo* crypt quantification of small intestinal 6-day-old EnO from SAMPDex-25, SAMP-5, and AKR-5 mice. Scale bars, 100 μm.

(G) *De novo* crypt quantification of small intestinal 6-day-old EnO from AKR-25, SAMP-25, and SAMPDex-25 mice. Scale bars, 100 μm.

(H–L) (H) OLFM4 and (I) LYSOZYME staining of AKR-25, SAMP-25, and SAMPDex-25 small intestinal crypts. Scale bars, 50 μm. Frequency of live and dead CBC stem cells (Epcam$^+$ Ephb2^{hi}/CD44^{hi}GRP78^{low}/CD166$^+$ CD24^{med}/CD31$^-$CD45$^-$) and Paneth cells (CD24^{hi}UEA$^+$/CD31$^-$CD45$^-$) isolated from (J) crypts and (K) EnOs of AKR-25, SAMP-25, and SAMPDex-25 mice. Relative expression of indicated genes measured in (L) total tissue or in (M) EnOs. The mRNA levels were determined by qRT-PCR, normalized to β-actin and expressed as fold change ($2^{-\Delta\Delta Ct}$).
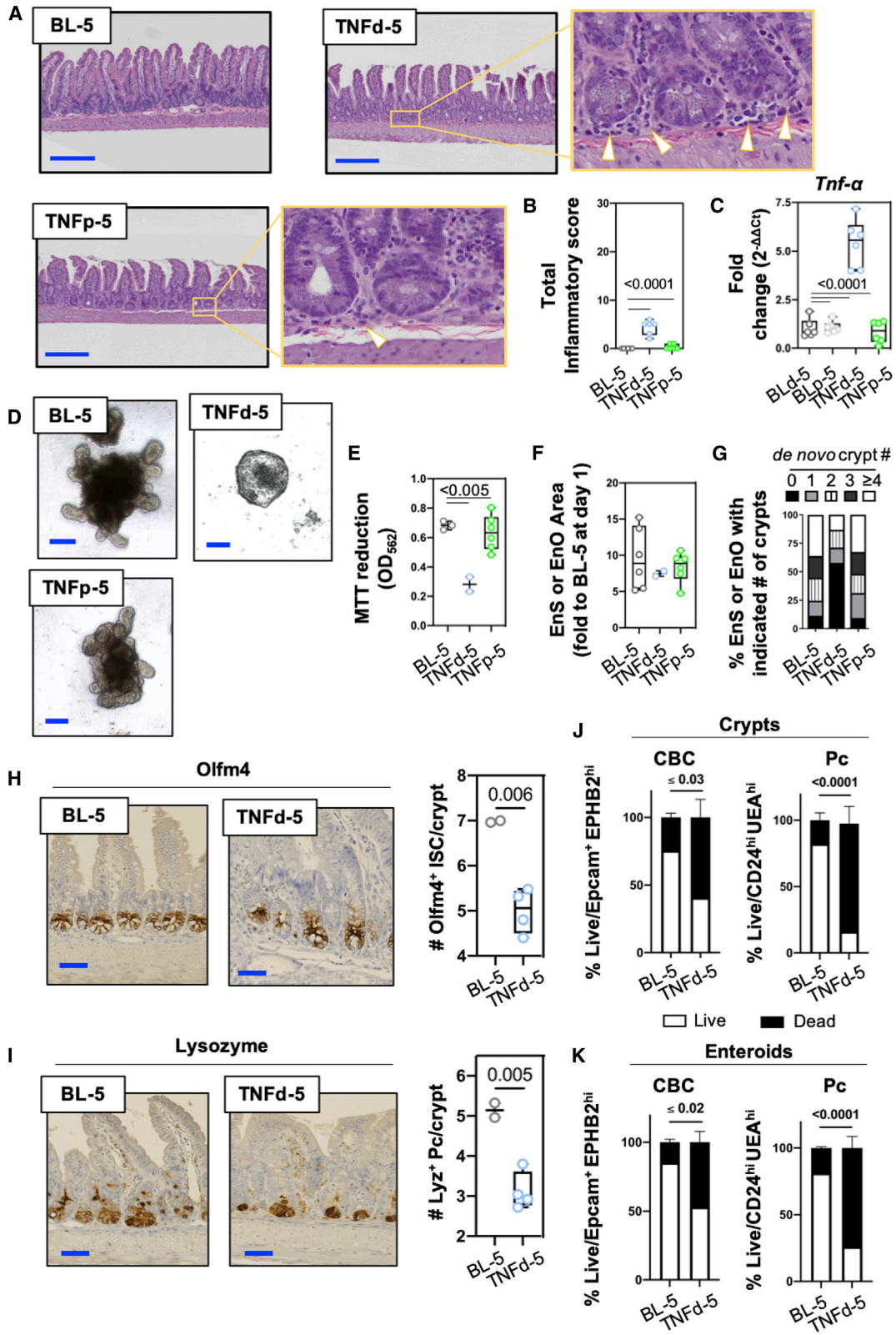
(legend on next page)

to CnO formation (Figures S3D–S3F). In this context, our data collectively suggest that crypts of highly inflamed ileal tissues from TNF mice are unable to form organoid structures and this correlated to the high TNF expression and reduced viability of ISCs and Paneth cells.

DISCUSSION

In this study, we developed a translationally relevant EnO-based model from ileitis-prone mice that recapitulate the epithelial cell phenotype of CD-like ileitis, and can be used to study IEBD in experimental CD and to identify and test novel therapies to correct this defect. Our study demonstrates that EnOs obtained from non-inflamed parental control mice resemble the 3D morphology of a healthy gut, while those from inflammation-free (but CD predisposed) 5-week-old SAMP mice display impaired formation. The Olson et al. study had demonstrated that SAMP mice develop a significant small intestine epithelial barrier dysfunction at a very early age, which precedes the onset of intestinal inflammation. Multiple studies in other animal models of IBD, including IL-10^{−/−} (Madsen et al., 2001) and mdr1a^{−/−} mice (Resta-Lenert et al., 2005), and in human studies have provided strong supporting evidence for epithelial barrier dysfunction preceding the onset of intestinal inflammation, thus suggesting a prominent role for IEBD early in disease development. Notably, inflammation-free SAMP EnOs produced an exacerbated expression profile of genes involved in epithelial secretory cell functions and a proinflammatory secreted cytokine profile. The exacerbated expression and cytokine profile, which is maintained in *ex vivo* expanded epithelial organoids from 5-week-old SAMP mice, demonstrates that SAMP EnOs recapitulate reactive epithelial changes specific of experimental CD. This aspect is of paramount importance as it emphasizes the physiologically relevant value of organoids generated from the SAMP mice model, rather

than those originated from healthy individuals, to mimic CD-like ileitis. This culture system holds exciting translational value since it may be used as an *in vivo* and *in vitro* drug-screening platform to test for therapies that can correct IEBD. Furthermore, multiple other immune-mediated diseases, such as celiac disease, type 1 diabetes (Odenwald and Turner, 2017), and nonalcoholic steatohepatitis (Luther et al., 2015) have been associated with IEBD and, thus, our model system provides a relevant platform to test therapies in the context of various disease states. Previous studies have used gastrointestinal organoids isolated from healthy donors to study infectious diseases, e.g., *Salmonella typhimurium* or *Clostridium difficile* (Leslie et al., 2015; Zhang et al., 2014); however, these models hold limited biological relevance for the study of CD, a complex and progressive inflammatory disease associated with more than 200 susceptibility loci (Liu et al., 2015). Our EnO model system is ideally suited to perform functional studies of host epithelium-microbial interactions in experimental CD.

Our study demonstrated that a highly inflammatory environment, such as the ileal milieu of 25-week-old SAMP mice and that of the distal ileum of TNF mice, impedes EnO formation, and that this is in stark contrast to the functional organoid formation seen in the same mice using non-inflamed tissues (e.g., colon), or in tissues from younger, "non-inflamed" mice (i.e., before ileitis onset). Intuitively, this makes sense as excessive cell death has been demonstrated in the lamina propria of highly inflamed areas in mice models and patients with CD (Blander, 2016; Grabinger et al., 2014; Kontoyiannis et al., 2002; Roulis et al., 2011). The role of inflammation in shaping the ISC niche is increasingly being recognized, with recent studies suggesting a crosstalk between immune cells and ISCs (Naik et al., 2018; Roulis et al., 2016). For instance, in one recent landmark study, Biton et al. (2018) demonstrated that the interaction of ISCs with T helper cells determines their fate with proinflammatory

Figure 6. Crypts from the Distal Ileum of Low-Grade Inflamed TNF Mice Form Rudimentary EnOs
Data are indicated as mean ± SD. The distal parts of the ileum of three TNF-5 mice were pooled together and two independent experiment were carried out. Whereas, two mice/group were used to generate TNFp-5 and BL-5 data, in three independent experiments.
(A) Representative photomicrographs of ileal sections from 5-week-old C57BL/6 (BL-5) and of the distal ileum (TNFd-5) and proximal small intestine (TNFp-5) from 5-week-old TNF mice. Scale bars, 200 μm. Zoomed images are at 20× magnification.
(B) Total inflammatory score of ileal tissue from BL-5 (0.0 ± 0.0), TNFd-5 (4.3 ± 1.4), and TNFp-5 (0.3 ± 0.5) mice.
(C) Relative expression of *Tnf-α* mRNA measured in total tissue RNA extracted from TNFd-5, TNFp-5 ilea, and from the distal and proximal portion of the ileum of BL-5 mice (BLd-5 and BLp-5, respectively). The mRNA levels were determined by qRT-PCR, normalized to β-actin and expressed as fold change ($2^{-\Delta\Delta Ct}$).
(D–G) (D) Growth, (E) viability, (F) size, and (G) *de novo* crypt quantification of small intestinal 6-day-old EnO from TNFd-5, TNFp-5, and BL-5 mice. Scale bars, 100 μm.
(H and I) (H) OLFM4 and (I) LYSOZYME staining of BL-5 and TNFd-5 small intestinal crypts. Scale bars, 50 μm. Frequency of live and dead CBC stem cells (Epcam^{+} Ephb2^{hi}/CD44^{hi}GRP78^{low}/CD166^{+} CD24[med]/CD31^{−}CD45^{−}) and Paneth cells (CD24^{hi}UEA^{+}/CD31^{−}CD45^{−}) isolated from (J) crypts and (K) EnOs of BL-5 and TNFd-5 mice.
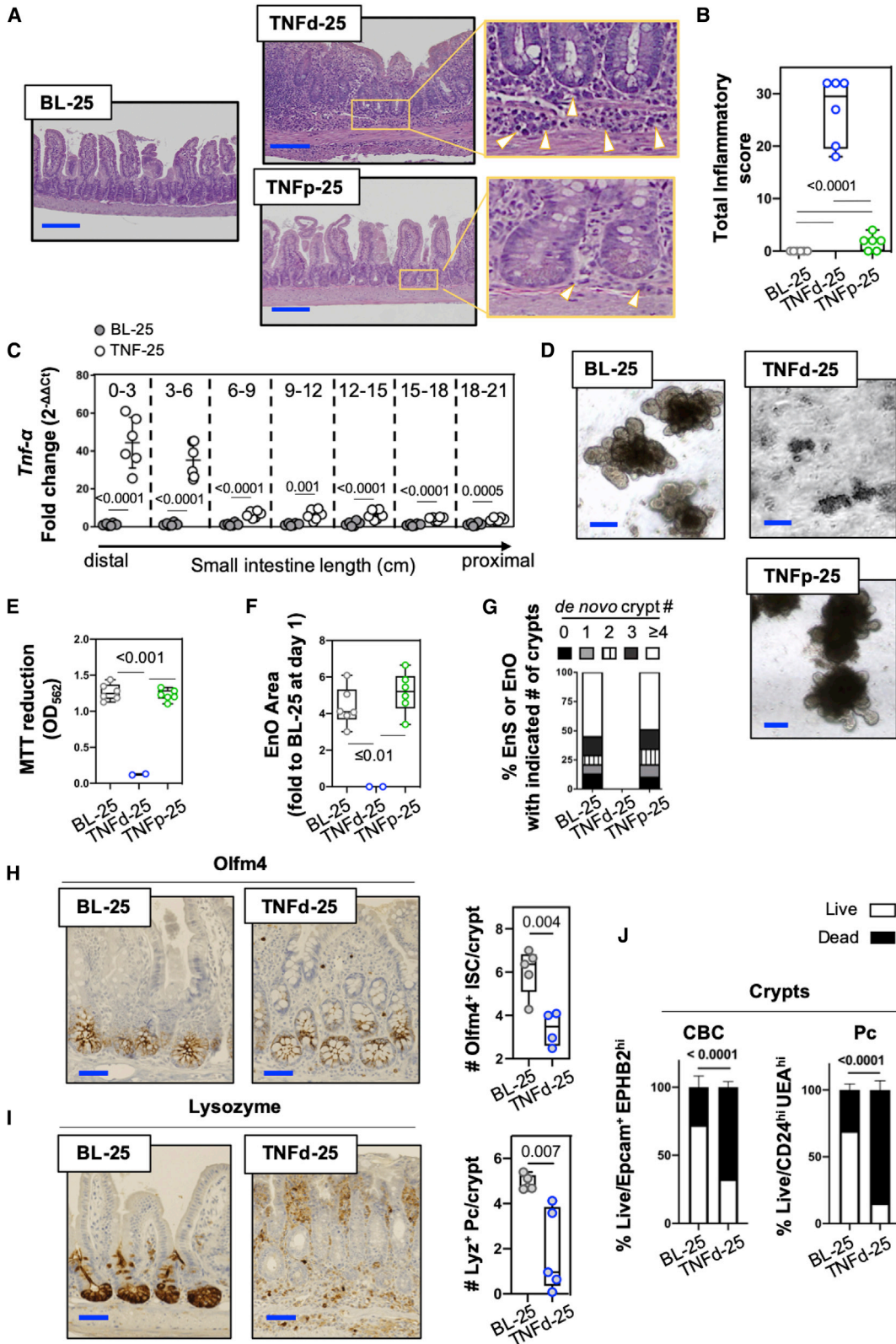
(legend on next page)

Th1, Th2, and Th17 cells and their cytokines, guiding a specific ISC differentiation and depletion/destruction, whereas co-culture with anti-inflammatory T_{regs} or IL-10 promoted ISC renewal. To exclude the effect of immune cells on ISC differentiation, we passaged EnOs at least twice. Similar to the Biton study, we demonstrated that crypts from SAMP mice with established severe inflammation had markedly reduced number of viable ISCs and viable Paneth cells, and diminished ability to form EnOs. Furthermore, mitigating inflammation through steroid (dexamethasone) treatment improves EnO generation and enhances the survival/viability of Paneth cells and ISCs. In the TNF mice, a genetically driven model of CD that is characterized by a continuous, aberrant TNF production, the ability to form EnOs correlates with degree of inflammation and TNF expression, e.g., crypts obtained from distal ileum of 25-week-old TNF mice with highest histologic scores corresponding to highest levels of TNF expression and inability to form EnOs. Sustained TNF-α production is known for inducing apoptosis in IECs of CD patient and mouse models of CD (Blander, 2016; Kontoyiannis et al., 2002; Roulis et al., 2011) and dose-dependent cell death in organoids (Grabinger et al., 2014). Furthermore, similar to SAMP mice, severe inflammation markedly reduced the number of viable ISCs and Paneth cells in TNF mice. Therefore, our data shows that, in TNF mice, the high TNF levels that correspond with severe inflammation are responsible for EnO formation defect.

Our data from two murine models of experimental CD demonstrate that severe inflammation impairs the ability to form EnOs. However, the results from human studies to generate EnOs from inflamed areas of patients with CD patients have been mixed. Some studies demonstrate that the number and quality of isolated crypts from inflamed regions of CD and ulcerative colitis patients is too low to regularly form intestinal organoids (Dotti et al., 2017; Yoo and Donowitz, 2019). On the other hand, some studies report that the organoid-forming capacity is similar between inflamed and non-inflamed areas of CD patients and are similar to healthy controls (Dotti et al., 2017; Noben et al., 2017; Suzuki et al., 2018; VanDussen et al., 2015). We believe that, unlike our murine study, these studies have not utilized a standard scoring technique to quantify the degree of inflammation in the affected/inflamed areas of CD patients. Future studies using large numbers of CD patients with assessment of inflammation in diseased and non-diseased areas with correlation to EnO formation ability and medium conditions are warranted.

SAMP mice, even before the onset of ileitis, exhibit a primary alteration of epithelial function (Olson et al., 2006), especially Paneth cells, as we show in this study. A recent pivotal study by Kinchen et al. (2018) found dysregulation of the colonic ISC niche in ulcerative colitis patients and highlighted how the colitis milieu drives stem cell niche dysregulation and leads to impaired epithelial development and barrier dysfunction. Dissecting the molecular pathways mediating barrier protection and dysfunction in the ISC niche is crucial for identifying the EnO defect and for developing strategies to reverse IEBD. Therefore, we generated the first global gene expression profile analysis of the SAMP ISC niche, and identified multiple signaling pathways already altered in young mice before histological detection of inflammation, suggesting their potential implication in disease development. Among these, the EMT pathway, which was highly enriched in the SAMP ISC niche, is well known to be implicated in fibrosis, which is a feature of human CD as well as of ileitis in SAMP mice (Jiang et al., 2018; Scharl et al., 2015). The process of both stem cell self-renewal and differentiation is coordinated by many signaling pathways, such as Notch and Wnt. Aberrancies in genes belonging to such pathways and their expression levels can influence these processes, leading to loss of stemness and of intestinal homeostasis (Fevr et al., 2007; Ootani et al., 2009; Sato and Clevers, 2013). Even before inflammation development, the

Figure 7. Crypts from the Distal Ileum of Highly Inflamed TNF Mice do Not Form EnSs
Data are indicated as mean ± SD. The distal parts of the ileum of three TNF-25 mice were pooled together and two independent experiment were carried out. Whereas, two mice/group were used to generate TNFp-25 and BL-25 data in three independent experiments.
(A) Representative photomicrographs of ileal sections from 25-week-old C57BL/6 (BL-25) and of the ileum (TNFd-25) and proximal small intestine (TNFp-25) from 25-week-old TNF mice. Scale bars, 200 μm. Zoomed images are at 20× magnification.
(B) Total histologic score of ileal tissue from BL-25 (0.0 ± 0.0), TNFd-25 (26.8 ± 5.8), and TNFp-25 (1.7 ± 1.4) mice.
(C) Segmental differential expression of *Tnf* mRNA between the distal and proximal ileum of TNF-25 and BL-25 mice, with 7-fold higher expression of *Tnf* in the distal ileum (tissue at 3 cm from the distal part of the ileum versus that at 10 cm). The mRNA levels were determined by qRT-PCR, normalized to β-actin and expressed as fold change ($2^{-\Delta\Delta Ct}$).
(D–G) (D) Growth, (E) viability, (F) size, and (G) *de novo* crypt quantification of small intestinal 6-day-old EnO from TNFd-25, TNFp-25, and BL-25 mice. Scale bars, 100 μm.
(H–J) (H) OLFM4 and (I) LYSOZYME staining of BL-25 and TNFd-25 small intestinal crypts. Scale bars, 50 μm.
(J) Frequency of live and dead CBC stem cells (Epcam$^+$ Ephb2^{hi}/CD44^{hi}GRP78^{low}/CD166$^+$ CD24^{med}/CD31$^-$CD45$^-$) and Paneth cells (CD24^{hi}UEA$^+$/CD31$^-$CD45$^-$) isolated from crypts of BL-25 and TNFd-25 mice.

Wnt3a-signaling pathway was found depleted in the ISC niche of 5-week-old SAMP mice in our RNA-seq experiment, and in Paneth cells, a major source of Wnt (Sato et al., 2011a, 2011b; Sato et al., 2009), had decreased viability and functionality. These data are in agreement with the concept that Paneth cells constitute the key niche to support Lgr5^{+} stem cells (Sato et al., 2011a, 2011b). Using a high Wnt3a-enriched medium in 5-week-old SAMP mice with absence of inflammation, we were successful in partially rescuing EnO morphology *in vitro*. Enteroid morphology was only partially restored in 5-week-old SAMP mice because multiple pathways are defective in these mice. Another pathway highly activated in the SAMP ISC niche was the UPR signaling, which critically regulates intestinal epithelial stem cell differentiation (Heijmans et al., 2013) and affects the development of chronic inflammation (Kaser et al., 2008; Shkoda et al., 2007). UPR activation in IECs and immune cells has been shown to result in NF-κB-mediated induction and secretion of proinflammatory cytokines, such as IL-6 and TNF (Grootjans et al., 2016). Our data show that dexamethasone treatment of SAMP mice results in downregulating the expression of proinflammatory NF-κB and partial rescue of organoid formation. However, steroids such as dexamethasone are potent and broad immunosuppressive agents and likely mediate their effect through multiple pathways. Our future studies will focus on more specific approaches to modulate the UPR signaling pathway. Thus, an improved understanding of the relationship between stem cells and their niches will facilitate the *in vivo* manipulation of the niche to modulate endogenous stem cell function, yielding new and improved stem-cell-based therapies.

Finally, EnOs generated from two mouse models of CD have defective formation and they can be used as a preclinical model to understand the role of IEBD in CD pathogenesis and to develop and test novel therapies.

EXPERIMENTAL PROCEDURES

Detailed methods are provided in Supplemental Information.

Experimental Animals
Five- and 25-week-old male SAMP and TNF mice, and age/gender-matched AKR/J (AKR) and BL control mice were used.

Mouse Intestinal Organoid Isolation, Culture, and Passage
Intestinal crypts were cultured as described previously (Sato et al., 2009), and every 6 days- EnOs were passaged dissolving Matrigel in cold PBS. EnOs passaged twice were grown for an additional 6 days and then gene and protein expression and cytokine secretion were measured.

Organoid Measurement
The surface area of EnO horizontal cross-sections was measured by acquiring nine non-overlapping pictures representing approximately the whole area of a single Matrigel dome (Figures S1A and S1B) using an Olympus CKX53 inverted microscope, and then analyzed using ImageJ software.

Assessment of Crypt Viability via MTT Reduction
Organoid viability was assessed over time by MTT assay.

Histology and Immunohistochemistry
Tissue collection and preparation for histological evaluation and immunohistochemistry was carried out as described previously (Burns et al., 2001; Sato et al., 2011a, 2011b).

Scanning Electron Microscopy
EnO morphology and ultrastructure was analyzed using scanning electron microscopy (SEM).

Dexamethasone Treatment
Animals were treated with either dexamethasone (4 mg kg^{-1}, every 24 h, intraperitoneal, for 7 days) or saline solution, as control.

RNA Isolation, Reverse Transcription, and Real-Time PCR
Primers used are described in Table S5.

Cytokine Assays
Cytokine levels were measured in EnO supernatants using BD Cytometric Bead Array Mouse Inflammation Kit in accordance with the manufacturer's instructions.

LCM of ISC Niche and Sample Preparation for RNA-Seq
ISC niche was collected by LCM and sample preparation for RNA-seq was performed by BGI Tech (Beijing Genomic Institute, Shenzhen, China)

Data Analysis and Functional Analysis of DEGs
Data are available at GEO (Gene Expression Omnibus, accession number GSE124825).

Statistical Analysis
Statistical analysis was carried out with GraphPad Prism (version 6.0; GraphPad Software, San Diego, CA). For comparison between two groups, Student's two-tailed unpaired t test or Mann-Whitney test was used. For comparison between more than two groups one-way ANOVA test with Bonferroni as *post-hoc* test was applied. $p \leq 0.05$ was considered significant. Each data point corresponds to a single mouse. Data are reported as mean ± SD. Number of independent experiments is indicated in each figure legend. Each data point in the figure represents one mouse.

Data and Code Availability

Data are available at GEO (Gene Expression Omnibus, accession number GSE124825).

SUPPLEMENTAL INFORMATION

Supplemental Information can be found online at https://doi.org/10.1016/j.stemcr.2020.06.017.

AUTHOR CONTRIBUTIONS

ACKNOWLEDGMENTS

REFERENCES

Alkim, C., Alkim, H., Koksal, A.R., Boga, S., and Sen, I. (2015). Angiogenesis in inflammatory bowel disease. Int. J. Inflam. *2015*, 970890.

Barnes, P.J. (2017). Glucocorticosteroids. Handb. Exp. Pharmacol. *237*, 93–115.

Baumgart, D.C., and Sandborn, W.J. (2012). Crohn's disease. Lancet *380*, 1590–1605.

Baur, P., Martin, F.P., Gruber, L., Bosco, N., Brahmbhatt, V., Collino, S., Guy, P., Montoliu, I., Rozman, J., Klingenspor, M., et al. (2011). Metabolic phenotyping of the Crohn's disease-like IBD etiopathology in the TNF(DeltaARE/WT) mouse model. J. Proteome Res. *10*, 5523–5535.

Biton, M., Haber, A.L., Rogel, N., Burgin, G., Beyaz, S., Schnell, A., Ashenberg, O., Su, C.W., Smillie, C., Shekhar, K., et al. (2018). T helper cell cytokines modulate intestinal stem cell renewal and differentiation. Cell *175*, 1307–1320.e22.

Blander, J.M. (2016). Death in the intestinal epithelium-basic biology and implications for inflammatory bowel disease. FEBS J. *283*, 2720–2730.

Burns, R.C., Rivera-Nieves, J., Moskaluk, C.A., Matsumoto, S., Cominelli, F., and Ley, K. (2001). Antibody blockade of ICAM-1 and VCAM-1 ameliorates inflammation in the SAMP-1/Yit adoptive transfer model of Crohn's disease in mice. Gastroenterology *121*, 1428–1436.

Butto, L.F., Jia, L.G., Arseneau, K.O., Tamagawa, H., Rodriguez-Palacios, A., Li, Z., De Salvo, C., Pizarro, T.T., Bamias, G., and Cominelli, F. (2019). Death-domain-receptor 3 deletion normalizes inflammatory gene expression and prevents ileitis in experimental Crohn's disease. Inflamm. Bowel Dis. *25*, 14–26.

Dahlhamer, J.M., Zammitti, E.P., Ward, B.W., Wheaton, A.G., and Croft, J.B. (2016). Prevalence of inflammatory bowel disease among adults aged ≥18 years—United States, 2015. MMWR Morb. Mortal. Wkly Rep. *65*, 1166–1169.

Dave, M., Papadakis, K.A., and Faubion, W.A., Jr. (2014). Immunology of inflammatory bowel disease and molecular targets for biologics. Gastroenterol. Clin. North Am. *43*, 405–424.

Dotti, I., Mora-Buch, R., Ferrer-Picon, E., Planell, N., Jung, P., Masamunt, M.C., Leal, R.F., Martin de Carpi, J., Llach, J., Ordas, I., et al. (2017). Alterations in the epithelial stem cell compartment could contribute to permanent changes in the mucosa of patients with ulcerative colitis. Gut *66*, 2069–2079.

Durand, A., Donahue, B., Peignon, G., Letourneur, F., Cagnard, N., Slomianny, C., Perret, C., Shroyer, N.F., and Romagnolo, B. (2012). Functional intestinal stem cells after Paneth cell ablation induced by the loss of transcription factor Math1 (Atoh1). Proc. Natl. Acad. Sci. U S A *109*, 8965–8970.

Fatehullah, A., Tan, S.H., and Barker, N. (2016). Organoids as an in vitro model of human development and disease. Nat. Cell Biol. *18*, 246–254.

Fevr, T., Robine, S., Louvard, D., and Huelsken, J. (2007). Wnt/beta-catenin is essential for intestinal homeostasis and maintenance of intestinal stem cells. Mol. Cell Biol. *27*, 7551–7559.

Grabinger, T., Luks, L., Kostadinova, F., Zimberlin, C., Medema, J.P., Leist, M., and Brunner, T. (2014). Ex vivo culture of intestinal crypt organoids as a model system for assessing cell death induction in intestinal epithelial cells and enteropathy. Cell Death Dis. *5*, e1228.

Grootjans, J., Kaser, A., Kaufman, R.J., and Blumberg, R.S. (2016). The unfolded protein response in immunity and inflammation. Nat. Rev. Immunol. *16*, 469–484.

Heijmans, J., van Lidth de Jeude, J.F., Koo, B.K., Rosekrans, S.L., Wielenga, M.C., van de Wetering, M., Ferrante, M., Lee, A.S., Onderwater, J.J., Paton, J.C., et al. (2013). ER stress causes rapid loss of intestinal epithelial stemness through activation of the unfolded protein response. Cell Rep. *3*, 1128–1139.

Hemmerling, J., Heller, K., Hormannsperger, G., Bazanella, M., Clavel, T., Kollias, G., and Haller, D. (2014). Fetal exposure to maternal inflammation does not affect postnatal development of genetically-driven ileitis and colitis. PLoS One 9, e98237.

Jiang, H., Shen, J., and Ran, Z. (2018). Epithelial-mesenchymal transition in Crohn's disease. Mucosal Immunol. 11, 294–303.

Kaser, A., Lee, A.H., Franke, A., Glickman, J.N., Zeissig, S., Tilg, H., Nieuwenhuis, E.E., Higgins, D.E., Schreiber, S., Glimcher, L.H., and Blumberg, R.S. (2008). XBP1 links ER stress to intestinal inflammation and confers genetic risk for human inflammatory bowel disease. Cell 134, 743–756.

Kinchen, J., Chen, H.H., Parikh, K., Antanaviciute, A., Jagielowicz, M., Fawkner-Corbett, D., Ashley, N., Cubitt, L., Mellado-Gomez, E., Attar, M., et al. (2018). Structural remodeling of the human colonic mesenchyme in inflammatory bowel disease. Cell 175, 372–386.e17.

Kontoyiannis, D., Boulougouris, G., Manoloukos, M., Armaka, M., Apostolaki, M., Pizarro, T., Kotlyarov, A., Forster, I., Flavell, R., Gaestel, M., et al. (2002). Genetic dissection of the cellular pathways and signaling mechanisms in modeled tumor necrosis factor-induced Crohn's-like inflammatory bowel disease. J. Exp. Med. 196, 1563–1574.

Kontoyiannis, D., Pasparakis, M., Pizarro, T.T., Cominelli, F., and Kollias, G. (1999). Impaired on/off regulation of TNF biosynthesis in mice lacking TNF AU-rich elements: implications for joint and gut-associated immunopathologies. Immunity 10, 387–398.

Kosiewicz, M.M., Nast, C.C., Krishnan, A., Rivera-Nieves, J., Moskaluk, C.A., Matsumoto, S., Kozaiwa, K., and Cominelli, F. (2001). Th1-type responses mediate spontaneous ileitis in a novel murine model of Crohn's disease. J. Clin. Invest. 107, 695–702.

Kozaiwa, K., Sugawara, K., Smith, M.F., Jr., Carl, V., Yamschikov, V., Belyea, B., McEwen, S.B., Moskaluk, C.A., Pizarro, T.T., Cominelli, F., and McDuffie, M. (2003). Identification of a quantitative trait locus for ileitis in a spontaneous mouse model of Crohn's disease: SAMP1/YitFc. Gastroenterol. 125, 477–490.

Leslie, J.L., Huang, S., Opp, J.S., Nagy, M.S., Kobayashi, M., Young, V.B., and Spence, J.R. (2015). Persistence and toxin production by Clostridium difficile within human intestinal organoids result in disruption of epithelial paracellular barrier function. Infect. Immun. 83, 138–145.

Liu, J.Z., van Sommeren, S., Huang, H., Ng, S.C., Alberts, R., Takahashi, A., Ripke, S., Lee, J.C., Jostins, L., Shah, T., et al. (2015). Association analyses identify 38 susceptibility loci for inflammatory bowel disease and highlight shared genetic risk across populations. Nat. Genet. 47, 979–986.

Luther, J., Garber, J.J., Khalili, H., Dave, M., Bale, S.S., Jindal, R., Motola, D.L., Luther, S., Bohr, S., Jeoung, S.W., et al. (2015). Hepatic injury in nonalcoholic steatohepatitis contributes to altered intestinal permeability. Cell Mol. Gastroenterol. Hepatol. 1, 222–232.

Madsen, K., Cornish, A., Soper, P., McKaigney, C., Jijon, H., Yachimec, C., Doyle, J., Jewell, L., and De Simone, C. (2001). Probiotic bacteria enhance murine and human intestinal epithelial barrier function. Gastroenterology 121, 580–591.

Marini, M., Bamias, G., Rivera-Nieves, J., Moskaluk, C.A., Hoang, S.B., Ross, W.G., Pizarro, T.T., and Cominelli, F. (2003). TNF-alpha neutralization ameliorates the severity of murine Crohn's-like ileitis by abrogation of intestinal epithelial cell apoptosis. Proc. Natl. Acad. Sci. U S A 100, 8366–8371.

Middendorp, S., Schneeberger, K., Wiegerinck, C.L., Mokry, M., Akkerman, R.D., van Wijngaarden, S., Clevers, H., and Nieuwenhuis, E.E. (2014). Adult stem cells in the small intestine are intrinsically programmed with their location-specific function. Stem Cells 32, 1083–1091.

Naik, S., Larsen, S.B., Cowley, C.J., and Fuchs, E. (2018). Two to tango: dialog between immunity and stem cells in health and disease. Cell 175, 908–920.

Nefzger, C.M., Jarde, T., Rossello, F.J., Horvay, K., Knaupp, A.S., Powell, D.R., Chen, J., Abud, H.E., and Polo, J.M. (2016). A versatile strategy for isolating a highly enriched population of intestinal stem cells. Stem Cell Reports 6, 321–329.

Ng, S.C., Shi, H.Y., Hamidi, N., Underwood, F.E., Tang, W., Benchimol, E.I., Panaccione, R., Ghosh, S., Wu, J.C.Y., Chan, F.K.L., et al. (2018). Worldwide incidence and prevalence of inflammatory bowel disease in the 21st century: a systematic review of population-based studies. Lancet 390, 2769–2778.

Noben, M., Verstockt, B., de Bruyn, M., Hendriks, N., Van Assche, G., Vermeire, S., Verfaillie, C., and Ferrante, M. (2017). Epithelial organoid cultures from patients with ulcerative colitis and Crohn's disease: a truly long-term model to study the molecular basis for inflammatory bowel disease? Gut 66, 2193–2195.

Odenwald, M.A., and Turner, J.R. (2017). The intestinal epithelial barrier: a therapeutic target? Nat. Rev. Gastroenterol. Hepatol. 14, 9–21.

Olson, T.S., Reuter, B.K., Scott, K.G., Morris, M.A., Wang, X.M., Hancock, L.N., Burcin, T.L., Cohn, S.M., Ernst, P.B., Cominelli, F., et al. (2006). The primary defect in experimental ileitis originates from a nonhematopoietic source. J. Exp. Med. 203, 541–552.

Ootani, A., Li, X., Sangiorgi, E., Ho, Q.T., Ueno, H., Toda, S., Sugihara, H., Fujimoto, K., Weissman, I.L., Capecchi, M.R., and Kuo, C.J. (2009). Sustained in vitro intestinal epithelial culture within a Wnt-dependent stem cell niche. Nat. Med. 15, 701–706.

Pizarro, T.T., Pastorelli, L., Bamias, G., Garg, R.R., Reuter, B.K., Mercado, J.R., Chieppa, M., Arseneau, K.O., Ley, K., and Cominelli, F. (2011). SAMP1/YitFc mouse strain: a spontaneous model of Crohn's disease-like ileitis. Inflamm. Bowel Dis. 17, 2566–2584.

Resta-Lenert, S., Smitham, J., and Barrett, K.E. (2005). Epithelial dysfunction associated with the development of colitis in conventionally housed mdr1a-/- mice. Am. J. Physiol. Gastrointest. Liver Physiol. 289, G153–G162.

Rodriguez-Palacios, A., Kodani, T., Kaydo, L., Pietropaoli, D., Corridoni, D., Howell, S., Katz, J., Xin, W., Pizarro, T.T., and Cominelli, F. (2015). Stereomicroscopic 3D-pattern profiling of murine and human intestinal inflammation reveals unique structural phenotypes. Nat. Commun. 6, 7577.

Roulis, M., Armaka, M., Manoloukos, M., Apostolaki, M., and Kollias, G. (2011). Intestinal epithelial cells as producers but not targets of chronic TNF suffice to cause murine Crohn-like pathology. Proc. Natl. Acad. Sci. U S A 108, 5396–5401.

Roulis, M., Bongers, G., Armaka, M., Salviano, T., He, Z., Singh, A., Seidler, U., Becker, C., Demengeot, J., Furtado, G.C., et al. (2016). Host and microbiota interactions are critical for development of murine Crohn's-like ileitis. Mucosal Immunol. *9*, 787–797.

Sato, T., and Clevers, H. (2013). Growing self-organizing mini-guts from a single intestinal stem cell: mechanism and applications. Science *340*, 1190–1194.

Sato, T., Stange, D.E., Ferrante, M., Vries, R.G., Van Es, J.H., Van den Brink, S., Van Houdt, W.J., Pronk, A., Van Gorp, J., Siersema, P.D., and Clevers, H. (2011a). Long-term expansion of epithelial organoids from human colon, adenoma, adenocarcinoma, and Barrett's epithelium. Gastroenterology *141*, 1762–1772.

Sato, T., van Es, J.H., Snippert, H.J., Stange, D.E., Vries, R.G., van den Born, M., Barker, N., Shroyer, N.F., van de Wetering, M., and Clevers, H. (2011b). Paneth cells constitute the niche for Lgr5 stem cells in intestinal crypts. Nature *469*, 415–418.

Sato, T., Vries, R.G., Snippert, H.J., van de Wetering, M., Barker, N., Stange, D.E., van Es, J.H., Abo, A., Kujala, P., Peters, P.J., and Clevers, H. (2009). Single Lgr5 stem cells build crypt-villus structures in vitro without a mesenchymal niche. Nature *459*, 262–265.

Scharl, M., Huber, N., Lang, S., Furst, A., Jehle, E., and Rogler, G. (2015). Hallmarks of epithelial to mesenchymal transition are detectable in Crohn's disease associated intestinal fibrosis. Clin. Transl Med. *4*, 1.

Severi, C., Sferra, R., Scirocco, A., Vetuschi, A., Pallotta, N., Pronio, A., Caronna, R., Di Rocco, G., Gaudio, E., Corazziari, E., and Onori, P. (2014). Contribution of intestinal smooth muscle to Crohn's disease fibrogenesis. Eur. J. Histochem. *58*, 2457.

Shkoda, A., Ruiz, P.A., Daniel, H., Kim, S.C., Rogler, G., Sartor, R.B., and Haller, D. (2007). Interleukin-10 blocked endoplasmic reticulum stress in intestinal epithelial cells: impact on chronic inflammation. Gastroenterology *132*, 190–207.

Stahn, C., Lowenberg, M., Hommes, D.W., and Buttgereit, F. (2007). Molecular mechanisms of glucocorticoid action and selective glucocorticoid receptor agonists. Mol. Cell Endocrinol. *275*, 71–78.

Stelzner, M., Helmrath, M., Dunn, J.C., Henning, S.J., Houchen, C.W., Kuo, C., Lynch, J., Li, L., Magness, S.T., Martin, M.G., et al. (2012). A nomenclature for intestinal in vitro cultures. Am. J. Physiol. Gastrointest. Liver Physiol. *302*, G1359–G1363.

Suzuki, K., Murano, T., Shimizu, H., Ito, G., Nakata, T., Fujii, S., Ishibashi, F., Kawamoto, A., Anzai, S., Kuno, R., et al. (2018). Single cell analysis of Crohn's disease patient-derived small intestinal organoids reveals disease activity-dependent modification of stem cell properties. J. Gastroenterol. *53*, 1035–1047.

VanDussen, K.L., Marinshaw, J.M., Shaikh, N., Miyoshi, H., Moon, C., Tarr, P.I., Ciorba, M.A., and Stappenbeck, T.S. (2015). Development of an enhanced human gastrointestinal epithelial culture system to facilitate patient-based assays. Gut *64*, 911–920.

Vidrich, A., Buzan, J.M., Barnes, S., Reuter, B.K., Skaar, K., Ilo, C., Cominelli, F., Pizarro, T., and Cohn, S.M. (2005). Altered epithelial cell lineage allocation and global expansion of the crypt epithelial stem cell population are associated with ileitis in SAMP1/YitFc mice. Am. J. Pathol. *166*, 1055–1067.

Yoo, J.H., and Donowitz, M. (2019). Intestinal enteroids/organoids: a novel platform for drug discovery in inflammatory bowel diseases. World J. Gastroenterol. *25*, 4125–4147.

Zhang, Y.G., Wu, S., Xia, Y., and Sun, J. (2014). *Salmonella*-infected crypt-derived intestinal organoid culture system for host-bacterial interactions. Physiol. Rep. *2*, e12147.